J|A|C|S
ARTICLES
Published on Web 09/05/2002

The Spin Distribution in Low-Spin Iron Porphyrins

Mikael P. Johansson,*,† Dage Sundholm,†,‖ Gary Gerfen,‡,⊥ and Mårten Wikström§,#

Contribution from the Department of Chemistry, P.O. Box 55 FIN-00014, University of Helsinki, Finland, Department of Physiology and Biophysics, Albert Einstein College of Medicine, 1300 Morris Park Avenue, Bronx, New York 10461, and Helsinki Bioenergetics Group, Institute of Biotechnology, P.O. Box 65 FIN-00014 University of Helsinki, Finland

Received April 12, 2002

Abstract: In many low-spin ($S = {}^1/_2$) iron porphyrin derivatives, electron spin resonance (ESR) spectra indicate that one of the d_π orbitals of iron, either a d_{xz} or d_{yz}, depending on the axial ligands of the porphyrin complex as well as their orientation, is essentially singly occupied; the unpaired electron is almost completely located at the metal. In contrast, nuclear magnetic resonance (NMR) and electron nuclear double resonance (ENDOR) spectroscopy convincingly show that a significant share of the unpaired electron is delocalized. This apparent contradiction is explained by the present density-functional-theory (DFT) calculations performed on a heme *a* model as well as on bis-imidazole-ligated iron porphyrin without substituents. The calculations show that the integrated spin density at the iron atom is nearly one, in agreement with the ESR measurements. However, significant areas with opposite (β) spin are found along the Fe−N bond axes, thus evoking a need for additional α-spin density to be present in the porphyrin ring, ring substituents, and the axial ligands to keep the net amount of unpaired spin exactly one. The gross spin density, that is, the sum of unpaired α and β spins, amounts to about 1.3 electrons. It seems that the degree to which α and β spin dominate in different regions of the heme structure, as evidenced in these calculations, has not been previously observed.

I. Introduction

The spin of the electron[1,2] is today exploited by a number of different spectroscopic methods. Different properties such as molecular structures, electron configurations of transition metals, and spin-density distributions of paramagnetic, that is, open-shell molecules, can thus be deduced. The most popular spectroscopic methods for studies of paramagnetic biomolecules are electron spin resonance (ESR), and nuclear magnetic resonance (NMR) spectroscopy. ESR spectroscopy is used to derive electronic *g*-tensors and magnetic hyperfine interactions. For hemes, the *g*-tensors mainly provide the orbital occupation of the iron,[3−7] whereas the spin densities can be estimated from the isotropic and anisotropic hyperfine-interaction constants.[7−9] NMR spectroscopy on paramagnetic molecules provides information about the spin-density distribution and indirectly about the electron configuration of the metal. By applying semiempirical models in the interpretation of the measured ESR and NMR spectra, information about the distribution of the unpaired electrons can be deduced from the experiment.[10−13] Mössbauer spectroscopy in the presence of a magnetic field can also provide magnetic hyperfine-coupling constants[14,15] and thereby spin densities.

For hemes, there is something of a controversy between, on one hand, the *g*-tensor deduction from ESR data and, on the other hand, the NMR spectra. The *g*-tensors seem to require almost one whole unpaired d_π electron at the iron, while the NMR spectra indicate that up to 0.2 unpaired electrons are dispersed in the porphyrin ring, the ring substituents, and the axial ligands.[16−18] More recent ESR measurements indicate that the spin density is indeed somewhat delocalized to the porphyrin ring[7,8,19,20] but also that almost one unpaired electron is confined

* To whom correspondence should be addressed. E-mail: mikael.johansson@helsinki.fi.
† Department of Chemistry, P.O. Box 55 FIN-00014, University of Helsinki.
‡ Albert Einstein College of Medicine.
§ Institute of Biotechnology, P.O. Box 65 FIN-00014 University of Helsinki.
‖ E-mail: Sundholm@chem.helsinki.fi.
⊥ E-mail: Gerfen@aecom.yu.edu.
E-mail: Marten.Wikstrom@helsinki.fi.

(1) Uhlenbeck, G. E.; Goudsmit, S. *Naturwissenschaften* **1925**, *47*, 953.
(2) Uhlenbeck, G. E.; Goudsmit, S. *Nature* **1926**, *117*, 264.
(3) Blumberg, W. E.; Peisach, J. *Adv. Chem. Ser.* **1971**, *100*, 271.
(4) Peisach, J.; Blumberg, W. E.; Adler, A. D. *Ann. N.Y. Acad. Sci.* **1973**, *206*, 310.
(5) Walker, F. A.; Reis, D.; Balke, V. L. *J. Am. Chem. Soc.* **1984**, *106*, 6888.
(6) McGarvey, B. R. *Coord. Chem. Rev.* **1998**, *170*, 75.
(7) Walker, F. A. *Coord. Chem. Rev.* **1999**, *185*−*186*, 471.
(8) Astashkin, A. V.; Raitsimring, A. M.; Walker, F. A. *J. Am. Chem. Soc.* **2001**, *123*, 1905, .
(9) Astashkin, A. V.; Raitsimring, A. M.; Kennedy, A. R.; Shokhireva, T. K.; Walker, F. A. *J. Phys. Chem. A* **2002**, *106*, 74.
(10) McConnell, H. M.; Chesnut, D. B. *J. Chem. Phys.* **1958**, *28*, 107.
(11) Kaiser, E. T., Kevan, L. Eds. *Radical Ions*; Wiley-Interscience: New York, 1968.
(12) Bertini, I.; Luchinat, C.; Parigi, G. *Eur. J. Inorg. Chem.* **2000**, *2473* 2000.
(13) Bertini, I.; Luchinat, C.; Parigi, G. *Solution NMR of Paramagnetic Molecules*; Elsevier: Amsterdam, 2001.
(14) Oosterhuis, W. T.; Lang, G. *Phys. Rev.* **1969**, *178*, 439.
(15) Taylor, C. P. S. *Biochim. Biophys. Acta* **1977**, *491*, 137.
(16) Horrocks, W. D.; Greenberg, E. S. *Biochim. Biophys. Acta* **1973**, *322*, 38.
(17) Goff, H. M. *J. Am. Chem. Soc.* **1981**, *103*, 3714.
(18) Tan, H.; Simonis, U.; Shokhirev, N. V.; Walker, F. A. *J. Am. Chem. Soc.* **1994**, *116*, 5784.
(19) Scholes, C. P.; Falkowski, K. M.; Chen, S.; Bank, J. *J. Am. Chem. Soc.* **1986**, *108*, 1660.
(20) Shokhirev, N. V.; Walker, F. A. *J. Phys. Chem.* **1995**, *99*, 17795.

to the iron d_π orbitals. Horrocks and Greenberg[16] attributed the apparent contradiction to inadequacies in the theory, a statement which in a way is vindicated here. Other ESR and NMR studies have also shown that spin density to some extent delocalizes to the surrounding parts of the molecule.[7,8,19−22] The extent of this spin delocalization is not very accurately known.[16,23,24] Judging from the available spectroscopic data, the spin delocalization seems to be quite dependent on the occupation of the electronic states at the iron and on the ligands.[7,25]

The most accurate means of obtaining detailed information about the spin-density distribution is to perform quantum chemical calculations. This is not a completely trivial task, since the inclusion of electron correlation effects and the use of flexible basis sets are absolutely necessary for quantitative calculations of, for example, hyperfine-interaction constants.[26−33] Recent DFT calculations[34−39] on transition metal compounds have shown that DFT calculations can provide hyperfine-coupling constants in fair agreement with experimental results. More general density functional studies of the spin-density distribution have also recently been performed.[38,40−43] Spin-density distributions obtained at the DFT level are generally more accurate than calculated isotropic hyperfine-coupling constants that sample only the nuclear positions. The accuracy of the spin densities must be much higher when sampling just one point in space instead of a larger region. Furthermore, when calculating the spin density at the atomic nucleus, which happens to be the most poorly described point when employing Gaussian basis functions, the difficulties that can appear in the calculations are easily understood.

Computational ab initio and DFT methods for calculation of electronic *g*-tensors have recently been developed and implemented.[44−51] However, to our knowledge, no quantitative and systematic calculations of NMR spectra of paramagnetic molecules at either ab initio or density-functional levels of theory have been reported.

On the basis of experimental observations, three types of low-spin hemes can be identified.[7] Types I and II formally have the unpaired electron in the d_π orbitals on iron, whereas for the type III hemes the iron d_δ orbital is singly occupied. In this notation, one assumes that the porphyrin ring lies in the *xy* plane. The difference between the type I and II hemes appears in the orientation of the axial ligands. Heme *a* with parallel axial imidazole ligands belongs to type II.

Recently we studied the change in the charge and spin density upon reduction of heme *a* at the density-functional level of theory.[52] In this work, we apply the same density-functional approach concentrating on the details of the spin density of heme *a*. Heme *a* is the low-spin, bis-imidazole-ligated iron-porphyrin cofactor in many of the respiratory heme−copper oxidases catalyzing most of the biological consumption of O_2. In the present heme *a* model, the propionate substituents are protonated, and the long hydroxyethylfarnesyl side chain is truncated to a hydroxyethyl group. The computational methods are also applied on a heme *a* model system whose porphyrin substituents are replaced by hydrogens. All systems considered have one net unpaired electron ($S = {}^1/_2$) and a charge of +1.

II. Methods

The molecular structure and the spin density of the low-spin, bis-imidazole-ligated porphyrins have been calculated at the spin-unrestricted density functional theory (UDFT) level using both a gradient-corrected local-density approximation (BP)[53−55] and a hybrid functional (B3LYP).[53,56−58] Since the Becke−Perdew (BP) functional does not contain any explicit Hartree−Fock exchange interaction terms, the resolution of the identity (RI) approximation of the Coulomb interaction can be employed.[59] The RI-DFT calculations are much faster than ordinary DFT calculations without any significant loss of accuracy.

All quantum chemical calculations were performed with the TURBOMOLE program package[60] using its standard split-valence (SV(P)) and triple-ζ valence (TZVP) basis sets[59,61,62] augmented with polarization functions. The TZVP basis set has polarization functions on all atoms, while the SV(P) basis set lacks polarization functions on the hydrogens. No symmetry restrictions were used in the calculations.

The spin density is obtained as the difference between the α and β spin contributions to the total electron density. We follow the normal convention that the number of α electrons is defined to be greater than the number of β electrons. The spin density was studied by evaluating it in a discrete distribution of equidistant Cartesian grid points. The radial distribution of the spin density was explicitly obtained by performing numerical integration of the angular dependence of the spin density in the discrete representation. The total accumulated spin density

(21) Mun, S. K.; Mallick, M. K.; Mishra, S.; Chang, J. C.; Das, T. P. *J. Am. Chem. Soc.* **1981**, *103*, 5024.
(22) Magliozzo, R. S.; Peisach, J. *Biochemistry* **1992**, *31*, 189.
(23) Rigby, S. E. J.; Moore, G. R.; Gray, J. C.; Gadsby, P. M. A.; George, S. J.; Thomson, A. J. *Biochem. J.* **1988**, *256*, 571.
(24) Axe, F. U.; Flowers, C.; Loew, G. H.; Waleh, A. *J. Am. Chem. Soc*. **1989**, *111*, *7333*.
(25) Kaufman, J.; Spicer, L. D.; Siegel, L. M. *Biochemistry* **1993**, *32*, 2853.
(26) Rassolov, V. A.; Chipman, D. M. *Theor. Chim. Acta* **1994**, *88*, 339.
(27) Engels, B. *Theor. Chim. Acta* **1993**, *86*, 429.
(28) Feller, D.; Davidson, E. R. *J. Chem. Phys*. **1988**, *88*, 7580.
(29) Stanton, J. F. *J. Chem. Phys*. **1994**, *101*, 371.
(30) Szalay, P. G.; Gauss, J. *J. Chem. Phys*. **1997**, *107*, 9028.
(31) Carmichael, I. *J. Phys. Chem. A* **1997**, *101*, 4633.
(32) Engels, B.; Eriksson, L. A.; Lunell, S. *Adv. Quantum Chem*. **1996**, *27*, 298.
(33) Kaupp, M. *Biochemistry* **2002**, *41*, 2895.
(34) Munzarová, M.; Kaupp, M. *J. Phys. Chem. A* **1999**, *103*, 9966.
(35) Munzarová, M.; Kubácek, P.; Kaupp, M. *J. Am. Chem. Soc*. **2000**, *122*, 11900.
(36) Sinnecker, S.; Koch, W.; Lubitz, W. *Phys. Chem. Chem. Phys*. **2000**, *2*, 4772.
(37) Larsen, S. C. *J. Phys. Chem. A* **2001**, *105*, 8333.
(38) García, J. I.; Medina, M.; Sancho, J.; Alonso, P. J.; Gómez-Moreno, C.; Mayoral, J. A.; Martínez, J. I. *J. Phys. Chem. A 106* **2002**, 4729.
(39) Ghosh, A.; Vangberg, T.; Gonzales, E.; Taylor, P. *J. Porphyrins Phthalocyanines* **2001**, **5**, 345.
(40) Rovira, C.; Kunc, K.; Hutter, J.; Ballone, P.; Parinello, M. *J. Phys. Chem. A* **1997**, *101*, 8914.
(41) Segall, M. D.; Payne, M. C.; Ellis, S. W.; Tucker, G. T.; Boyes, R. N. *Phys. Rev. E* **1998**, *57*, 4618.
(42) Segall, M. D.; Payne, M. C.; Ellis, S. W.; Tucker, G. T.; Boyes, R. N. *Chem. Res. Toxicol* **1998**, *11*, 962.
(43) Harris, D. L. *Curr. Opin. Chem. Biol*. **2001**, *5*, 724.
(44) Lushington, G. H.; Grein, F. *Int. J. Quantum Chem*. **1995**, *55*, 377.
(45) Schreckenbach, G.; Ziegler, T. *J. Phys. Chem. A* **1997**, *101*, 3388.
(46) van Lenthe, E.; Wormer, P. E. S.; van der Avoird, A. *J. Chem. Phys*. **1997**, *107*, 2488.
(47) Jayatilaka, D. *J. Chem. Phys*. **1998**, *108*, 7587.
(48) Engström, M.; Minaev, B.; Vahtras, O.; Ågren, H. *Chem. Phys*. **1998**, *237*, 149.
(49) Engström, M.; Himo, F.; Gräslund, A.; Minaev, B.; Vahtras, O.; Ågren, H. *J. Phys. Chem. A* **2000**, *104*, 5149.
(50) Patchkovskii, S.; Ziegler, T. *J. Am. Chem. Soc*. **2000**, *122*, 3506.
(51) Malkina, O. L.; Vaara, J.; Schimmelpfennig, B.; Munzarová, M.; Malkin, V. G.; Kaupp, M. *J. Am. Chem. Soc*. **2000**, *122*, 9206.
(52) Johansson, M. P.; Blomberg, M. R. A.; Sundholm, D.; Wikström, M. *Biochim. Biophys. Acta* **2002**, *1553*, 183.
(53) Vosko, S. H.; Wilk, L.; Nusair, M. *Can. J. Phys* **1980**, *58*, 1200.
(54) Perdew, J. P. *Phys. Rev. B* **1986**, *33*, 8822.
(55) Becke, A. D. *Phys. Rev. B* **1988**, *38*, 3098.
(56) Becke, A. D. *J. Chem. Phys*. **1993**, *98*, 5648.
(57) Lee, C.; Yang, W.; Parr, R. G. *Phys. Rev. B* **1988**, *37*, 785.
(58) Stephens, P. J.; Devlin, F. J.; Chabalowski, C. F.; Frisch, M. J. *J. Phys. Chem*. **1994**, *98*, 11623.
(59) Eichkorn, K.; Treutler, O.; Öhm, H.; Häser, M.; Ahlrichs, R. *Chem. Phys. Lett*. **1995**, *240*, 283.
(60) Ahlrichs, R.; Bär, M.; Häser, M.; Horn, H.; Kölmel, C. *Chem. Phys. Lett*. **1989**, *162*, 165.
(61) Schäfer, A.; Horn, H.; Ahlrichs, R. *J. Chem. Phys*. **1992**, *97*, 2571.
(62) Schäfer, A.; Huber, C.; Ahlrichs, R. *J. Chem. Phys*. **1994**, *100*, 5829.

inside a sphere with radius r, denoted by $\rho_{spin}(r)$, can then be obtained as

$$\rho_{spin}(r) = \frac{1}{N(r)} \frac{4}{3} \pi r^3 \sum_{i}^{N(r)} \rho_{spin,i} \quad (1)$$

where $N(r)$ is the number of integration points inside the sphere and $\rho_{spin,i}$ is the calculated spin density at grid point i. To improve the accuracy of the numerical integration, the deep core orbitals of the heavy atoms (1s for C, N, and O, as well as 1s, 2s, and 2p for Fe) were not considered.

III. Result and Discussion

III. A. Molecular Structures. The described computational methods have been applied on low-spin heme models. The molecular structure of the oxidized heme *a* molecule was optimized at the UDFT level without constraints, starting from the crystal structure.[63] In the model, a hydroxyethyl group replaces the long hydroxyethylfarnesyl side chain, and the propionate substituents are protonated, thus yielding a total molecular charge of +1. Both the BP[53−55] and the B3LYP[53,56−58] functionals with SV(P) and TZVP quality basis sets[59,61−62] were employed. At the BP level, the structure was also optimized with the TZVPP basis set.[62,64]

The molecular structures obtained at the BP-UDFT and B3LYP-UDFT levels of theory are rather similar. Slightly different orientations of the axial imidazole ligands seem to be favored by the different functionals; B3LYP/TZVP aligns the imidazoles almost in line with the meso carbons, whereas at the BP/TZVP level the imidazoles are aligned, but form a 10° angle with the meso carbons. Small deviations in the imidazole torsion angle result in very small energy differences. The BP/TZVPP-optimization gave an angle of 8°. Due to the deformed nature of the crystal structure, an unambiguous definition of the angle is difficult. The two imidazoles are oriented at slightly different angles of about 2 and 14°.

The Fe−N bonds are slightly longer at the B3LYP level, but never by more than 0.02 Å. At the B3LYP/TZVP level the porphyrin Fe−N_P distances are 2.02−2.03 Å while the Fe−N_{Im} is 2.02 Å. At the BP/TZVP level the respective distances are 2.00−2.03 and 2.00 Å. This can be compared to the average of the experimental distances for six-coordinated low-spin iron complexes of 1.986 and 1.983 Å.[65]

Compared with the initial crystal structure, the largest deviations are found in the orientation of the propionates, as well as in the tilt of the axial imidazoles; since the imidazoles are not anchored in the model, they can relax forming a right angle to the heme plane. The superimposed molecular structures of the optimized heme *a* model obtained at the B3LYP level using the TZVP basis set and the X-ray structure are shown in Figure 1. The Cartesian coordinates of both BP and B3LYP optimized models are available on our Internet page[66] and from the Journal as Supporting Information.

III. B. Spin Densities. The spatial spin-density distribution for heme *a* obtained at the B3LYP/TZVP level is shown in Figure 2. Excess α spin density is found in the blue areas, whereas the red areas represent excess β spin. The excess of α spin is mainly found at the central iron atom, but a notable amount of α spin is also located at the pyrrole carbons and in the vinyl unit. The formyl oxygen also has a small excess of α electrons. The most striking feature is the significant excess of β spin along the Fe−N bonds of the iron-ligating nitrogens. Although experimental evidence has been presented for the presence of β spin at the nitrogen nucleus, the present calculations clarify the extent and importance of spin polarization effects along the entire Fe−N bond. To our knowledge this has not been previously reported.

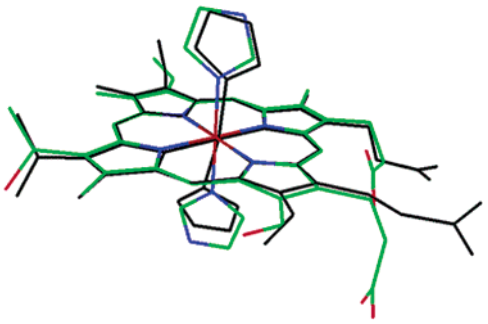

Figure 1. Structure of heme *a* optimized at the B3LYP UDFT level using the TZVP quality basis set (multicolor) superimposed on the crystal structure (black). The initial coordinates for cytochrome *c* oxidase from bovine heart mitochondria were taken from the Protein Data Bank[96] under the PDB identifier 2OCC.[63] Hydrogens are omitted.

The large excess of α spin on the iron atom leads to a spin polarization of the electron density outside the iron, which appears as an excess of β electrons. This can be considered as a large-scale, molecular version of the spin-polarization mechanism observed for atoms. In atoms, the unpaired valence electron polarizes the core shells. The polarization of the core orbitals leads to different amounts of α and β spin at the nucleus, which is reflected in the isotropic hyperfine-coupling constant. However, since the orbitals are normalized, the spin polarization must also result in a slightly more diffuse core orbital for the opposite spin. Thus, in atoms, the spin polarization is not only seen as a tiny spin difference at the nucleus, but also as a slightly more diffuse density of the opposite spin. In the low-spin heme, there is a large excess of α electrons around the iron, and the spin polarization results analogously in a slight, diffuse, excess of β electrons just outside the iron.

The delocalization of the spin density can be illustrated by radial spin-density distribution functions with the iron at the center, see eq 1. Figures 3 and 4 show the integrated net spin density for heme *a* inside a sphere of a given radius from the central iron. The region with excess β spin is clearly seen as it decreases the amount of the net α spin density. A maximum for the accumulated α spin density coincides with the covalent radius of iron of 1.2 Å. Here the integrated spin density reaches a value of 0.9−1.0, depending on the density functional used, which means that almost one unpaired electron is confined to the iron. A closer study of the spin density in the vicinity of the iron reveals that the single unpaired spin in the present low-spin ferric hemes is largely localized to the d_{xz}, d_{yz} (d_π) orbitals of the iron. The electron in the d_π shell becomes paired on reduction of the heme to the ferrous state.[40,52,67−70]

(63) Yoshikawa, S.; Shinzawa-Itoh, K.; Nakashima, R.; Yaono, R.; Yamashita, E.; Inoue, N.; Yao, M.; Fei, M. J.; Libeu, C. P.; Mizushima, T.; Yamaguchi, H.; Tomizaki, T.; Tsukihara, T. *Science* **1998**, *280*, 1723.
(64) Dunning, T. H., Jr. *J. Chem. Phys.* **1989**, *90*, 1007.
(65) Scheidt, W. R.; Gouterman, M. in *Iron Porphyrins (Part 1)*; Lever, A. B. P., Gray, H. B., Eds.; Addison-Wesley: Reading, MA, 1983; p 89.
(66) http://www.chem.helsinki.fi/Research/supplements/.
(67) Rovira, C.; Carloni, P.; Parinello, M. *J. Phys. Chem. B* **1999**, *103*, 7031.

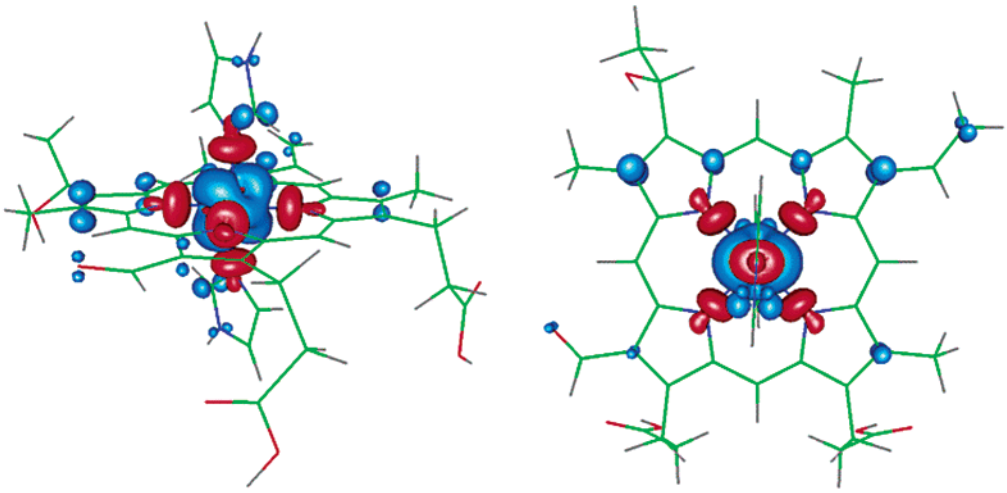

Figure 2. Side and top view of the spin distribution in heme *a*, calculated at the B3LYP/TZVP level. Blue regions have excess α density and red areas excess β density. The plot is created with gOpenMol.[97−99]

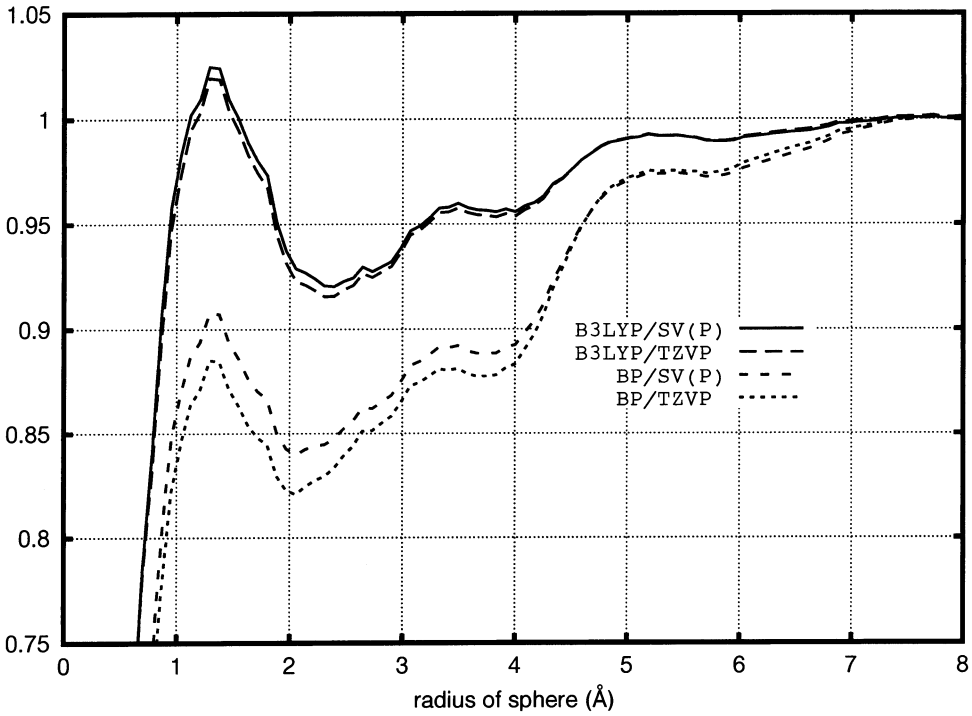

Figure 3. Effective α-spin density of heme *a* inside a sphere with a radius from 0 to 8 Å calculated with the BP and B3LYP functionals using the TZVP and SV(P) basis sets.

Outside the iron atom, near the ligating nitrogens, the excess of β electrons reduces the accumulated spin density by about 0.1 electron. Therefore, the net spin density reaches a minimum at a distance of 2 Å from the iron, at the ligating nitrogens. At about 3.5 Å the accumulated spin density has a small local maximum followed by a tiny minimum. For distances larger than 4 Å there is a fast increase in the accumulated spin density, and at about 7.5 Å all of the unpaired spin density has been found.

The accumulated spin-density distribution can be related to the molecular frame. The pyrrole α carbons (C_α) are located 3.1−3.2 Å from the iron atom. The meso carbons (C_{meso}) are at 3.5 Å, and the pyrrole β carbons (C_β) lie at a distance of about 4.2−4.4 Å from the iron. Figures 3 and 4 do not show it explicitly, but there are many small spin-density contributions of different sign. Between the nitrogens and the C_α atoms α spin dominates, whereas at C_{meso} there is a region with a small excess of β spin. Finally, the long spin-density tail seen in the curves comes mainly from the vinyl and formyl substituents.

The spin accumulation in the axial imidazoles was also calculated by explicit integration. Both imidazoles were found to possess almost identical amounts of unpaired spin, roughly 0.02 electrons of unpaired α together with 0.01 electrons of unpaired β. A separation of the contributions for spin delocal-

(68) Bertini, I.; Luchinat, C. *NMR of Paramagnetic Molecules in Biological Systems*; The Benjamin/Cummins Publ. Co.: Menlo Park, New York, 1986; pp 165.
(69) Goff, H. M. In *Iron Porphyrins (Part 1)*; Lever, A. B. P., Gray, H. B., Eds.; Addison-Wesley Publ. Co.; Reading, Mass., 1983; p 237.
(70) Palmer, G. In *Iron Porphyrins (Part 1)*; Lever, A. B. P., Gray, H. B., Eds.; Addison-Wesley Publ. Co.; Reading, Mass., 1983; p 43.

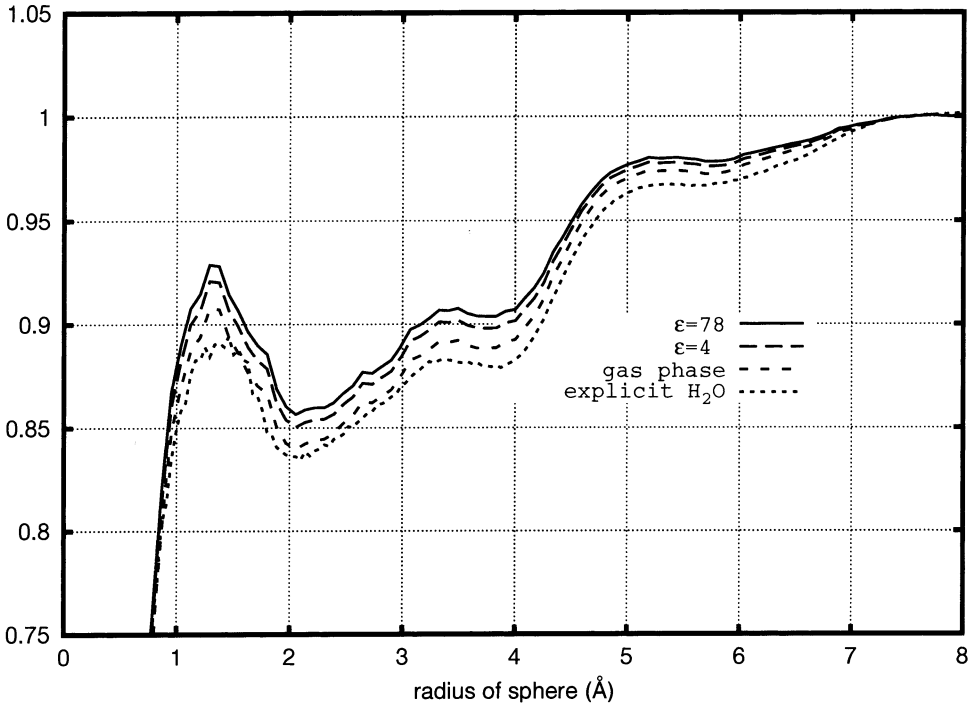

Figure 4. Effective α-spin density of heme *a* inside a sphere with a radius from 0 to 8 Å. Curves calculated for gas phase, for different values of the dielectric constant, and for explicit water solvation are shown. All curves are based on BP/SV(P) calculations.

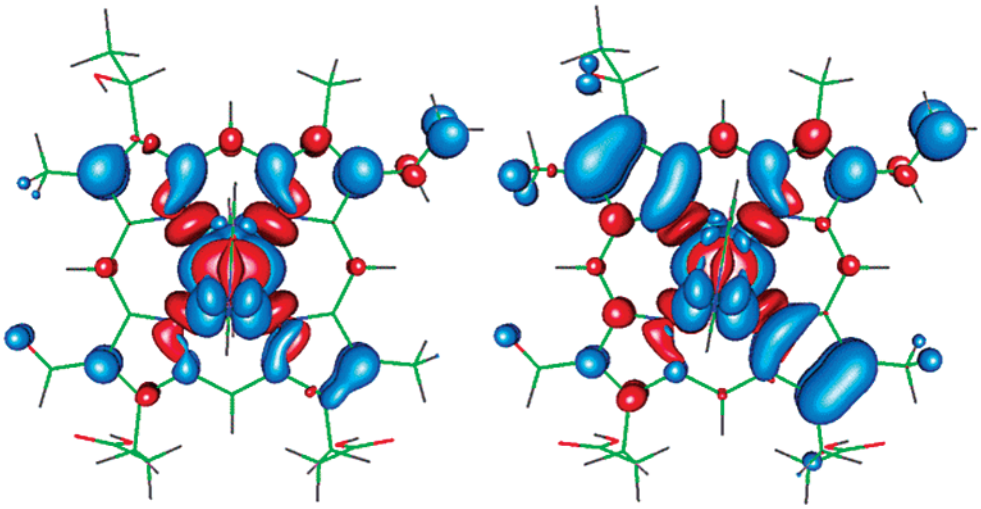

Figure 5. Finer details of α (blue) and *β* (red) spin density in heme *a* calculated at the B3LYP/TZVP (left) and BP/TZVP (right) levels on fully relaxed molecular structures.

ization outside the iron-ligated nitrogens between the porphyrin ring and the imidazoles is thus possible; about 0.1 unpaired electrons are found in the porphyrin macrocycle, while both imidazoles together have about 0.05 unpaired electrons. The definition of precisely which regions in space should be considered belonging to the imidazoles, and which to the macrocycle, is of course somewhat arbitrary.

The integration of all unpaired spin, that is, the sum of α- and *β*-spin densities, yields a total amount of 1.28−1.34 unpaired electrons in the low-spin heme model, calculated at the BP and B3LYP level, respectively. The main *β* spin-density contribution is not atom-centered. Instead, it appears along the Fe−N bonds and is rather diffuse. This aspect of the spin distribution cannot be accurately described by atom-centered population analyses. Single configuration methods based on the restricted open-shell approach must also fail since they, by definition, do not allow the presence of unpaired electrons with opposite spin. The widely used Hückel molecular orbital method belongs to this category. Although crude models often provide quick qualitative insights, there are no guarantees for their success. Since modern quantum chemistry software and hardware now allow rigorous studies on molecular systems of this size, there is no reason not to corroborate the cruder models with better calculations.

In Figure 5, the spin density has been plotted using a smaller threshold than in Figure 2, thus showing more details of the spin-density distribution. Both B3LYP (left side) and BP (right side) functionals show quite similar distributions of α and *β* spin excess. One can see that almost all carbons of the porphyrin macrocycle have some unpaired spin density in their vicinity.

At the C_β positions farther from the imidazole plane, the spin density is larger than for the other C_β atoms. Some of the α-carbons seem to lack spin density at the B3LYP-level. However, a lower plotting threshold reveals that they do have a very small β-spin excess. The vinyl group has spin density with opposite signs in π-type orbitals on both carbons.

A few differences between the B3LYP and BP spin distributions can be noted. At the B3LYP level, the propionates, one of the methyl groups, and the hydroxyethyl group lack unpaired spin, whereas at the BP level some unpaired spin is also found in the hydroxyethyl group and on one of the propionates. Furthermore, at B3LYP level, the meso carbon between the propionate chains fails to show any signs of spin density. The difference in the spin-density distributions obtained with the two density functionals is partly due to the difference in molecular structure, especially the different torsional angles of the imidazoles affect the results.

III. C. Comparison with Experiment. On the basis of their ENDOR experiments, Scholes et al.[19] proposed a presence of β-spin at the pyrrole nitrogens. This suggestion was later supported by electron spin−echo envelope modulation (ESEEM) spectroscopy measurements by Magliozzo and Peisach.[22] Further confirmation of the atomic spin-polarization effect for all the iron-ligated nitrogens is also given by this work; the spin density at the nuclei of the pyrrole nitrogens is −0.020 *e*, the imidazole N-1 nitrogens have a somewhat larger spin density of −0.024 *e*, where the negative sign denotes β spin. Goff[17] found experimentally that the meso carbons possess a slight excess of β-spin density, whereas excess α spin appears at the β-pyrrole carbons, α-pyrrole carbons, and at the pyrrole nitrogens. The notion that there is an excess of β spin at the meso carbons is supported by NMR determinations of proton hyperfine-coupling constants.[71,72] In later work, Turner[73] did not have to consider any β-spin density on the meso carbons in order to interpret the ^{13}C NMR spectrum for His-Met cytochrome *c*. These difficulties to interpret the spectroscopic data show that for molecules of this size it is all but trivial to obtain accurate spin densities from measured spectra.

Spectroscopic measurements of the isotropic coupling constants normally provide only the absolute value of the spin density at the nucleus. The sign of the isotropic hyperfine coupling relative to the dipolar coupling can be obtained from more sophisticated ENDOR and NMR studies. The spin density at the nucleus does not necessarily correlate with the spin-density distribution around it. BP and B3LYP calculations show a quite large excess of β spin of −0.11 electron at the iron nucleus, whereas α spin dominates in the surroundings. This observation is also made in solid-state calculations of the isotropic hyperfine-coupling constant for interstitial iron in silicon.[74]

A very thorough ENDOR examination of bis-imidazole-ligated low-spin ferric heme systems has been performed by Scholes et al.[19] Among other observations, they report inequivalence of pyrrole proton ENDOR signals in the studied tetraphenylporphyrin, $(TPP)Fe(Im)_2^+$, and attribute this to be a sign of an uneven π-electron spin distribution in the heme. A similar asymmetry was recently observed also by Hu et al.[75] In heme *a*, the pyrrole hydrogens are replaced by various substituents, but this of course does not prevent computational studies of the spin densities at the pyrrole carbons; the uneven spin distribution is clearly seen in Figure 2.

In Scholes study[19] on the symmetrically substituted $(TPP)Fe(Im)_2^+$ the spin density at the hydrogens of the meso carbons were found to be identical. For heme *a*, the calculated spin densities at the four meso carbons and hydrogens are similar, but small differences are noted. The meso carbons possess a slight excess of β electrons in their π-type orbitals. At the meso position between the propionate substituents, there is very little-to-no sign of spin density. The variations are an effect of the asymmetric substitution of the ring; the symmetrical unsubstituted heme model, treated in the next section, has identical spin densities in the meso positions. Both experiment and calculations find the spin density at the C-2 and C-5 carbons of the imidazole ligands to be very different.

ESR and NMR spectroscopy on paramagnetic molecules provide information about isotropic and anisotropic hyperfine-coupling constants. Spin densities at different atoms in the molecule can then be deduced from the measured hyperfine interaction. One of the aims of the ESR and NMR measurements to begin with, is to obtain the overall spin-density distribution. In the calculations, the hyperfine-coupling constants are very sensitive to the level of correlation treatment and the quality of the basis set, whereas the overall spin-density distribution is affected to a much lesser extent by the chosen computational level. Therefore, one should not concentrate the computational efforts solely on the calculation of hyperfine coupling constants, since the semiempirical models used for relating the spin-density distribution and the hyperfine coupling are not necessarily very accurate. A much more accurate description of the spin-density distribution is provided directly by the calculation. The calculated spin densities in combination with measured ESR and NMR spectra can provide improved models for an immediate interpretation of ESR and NMR spectra of paramagnetic molecules.

III. D. Substituent and Ligand Effects. To study the influence of the porphyrin substituents, the heme *a* structure was undressed so that it consisted of only the iron porphyrin ring with two axial imidazoles, $FeP(Im)_2^+$. Thus, hydrogens replaced all heme *a* substituents. For the heme system without porphyrin substituents, all the main features of the larger model are reproduced. Some differences in the details of the spin density can however be observed. The spin-density distributions in the porphyrin ring shows a much more symmetric distribution for the unsubstituted system than for heme *a*. The hole in the d shell also differs in orientation, being parallel with the plane defined by the axial imidazoles in $FeP(Im)_2^+$, whereas the hole in the heme *a* model is perpendicular to the imidazoles. The spin-density maxima appear at different C_β positions. This shows the importance of the ligands for the details of the spin distribution in hemes.

In heme *a*, the orientation of the axial imidazoles, in reality histidine residues, is fixed by the surrounding protein. In $FeP(Im)_2^+$ the imidazoles are free to rotate, and thus the effect of the orientation on the axial imidazoles was studied. The molecular structure optimization showed that perpendicular

(71) Shulman, R. G. Glarum, S. H.; Karplus, M. *J. Mol. Biol.* **1971**, *57*, 93.
(72) Turner, D. L. *Eur. J. Biochem.* **1993**, *211*, 563.
(73) Turner, D. L. *Eur. J. Biochem.* **1995**, *227*, 829.
(74) Weihrich, H.; Overhof, H. *Phys. Rev. B* **1996**, *54*, 4680.
(75) Hu, B.; Hauksson, J. B.; Tran, A. T. T.; Kolczak, U.; Pandey, R. K.; Rezzano, I. N.; Smith, K. M.; La Mar, G. N. *J. Am. Chem. Soc.* **2001**, *123*, 10063.

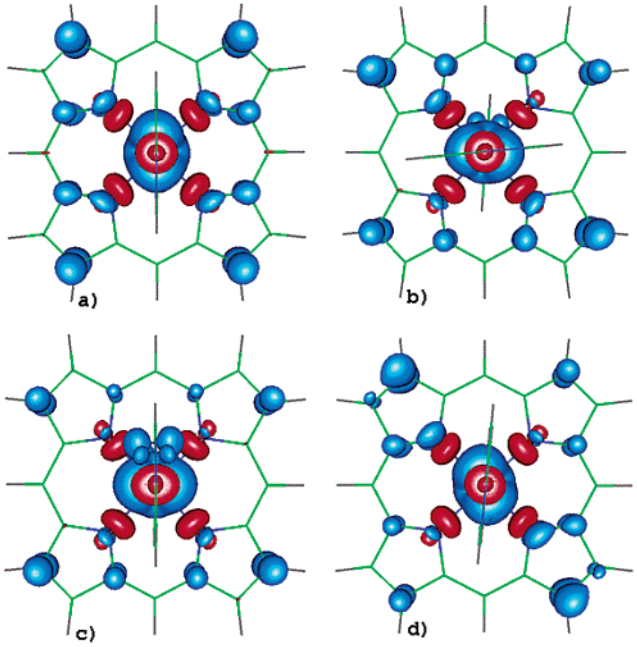

Figure 6. Top-view plots of the spin distribution for the unsubstituted heme model, $FeP(Im)_2^+$, with different orientations of the axial imidazoles: (a) parallel imidazoles, (b) perpendicular imidazoles (80° angle), (c) parallel imidazoles with both N-3's on the same side, (d) both imidazoles at an angle of 5°. The spin densities are calculated at the BP/SV(P) level using relaxed structures for (a), (b), and (c), while the structure of (d) is unrelaxed, constructed from (a).

imidazoles relax to form an 80° angle between the N-3 nitrogens. The porphyrin ring is also bent a bit out of the totally planar structure obtained with parallel imidazoles. The imidazoles seem to push the porphyrin ring away; an effect which is canceled when the imidazoles are parallel. That a repulsion and not an attraction is at play is more apparent in imidazole-ligated bacteriochlorophyll.[76] Since present-day density functionals cannot treat dispersion forces,[77] the ruffling must mainly be due to electrostatic, rather than van der Waals, interactions between the imidazoles and the porphyrin π electrons. However, this ruffling of the porphyrin ring together with the twisting of one imidazole ligand has almost no effect on the main features of the spin-density distribution. The parallel imidazole conformation with both of the N-3 nitrogens pointing in the same direction again has a planar porphyrin ring, but the spin-density distribution is rotated by 90° as compared to the conformation with parallel imidazoles and the N-3 nitrogens pointing in opposite directions.

Figure 6 shows the orientation of the hole in the d_π shell for the different cases studied. It is seen that the spin distribution in the heme plane follows the orientation of the spin density at the iron, that is, the occupation of the d_π orbitals. Spin densities on atoms parallel to the direction of the d orbital are strengthened at the expense of the spin densities at the other atoms in the porphyrin ring.[78] This line structure is very pronounced for the unsubstituted heme, but it is also clearly seen for the heme *a* model.

By defining the *x*- and *y*-axes to pass through the meso carbons in the heme plane, one can see that the unpaired electron at the iron occupies either d_{xz} or d_{yz}. The occupation of the orbitals is dictated by the orientation of the axial ligands and by the ring substituents. For FeP with two equivalent linear axial ligands, the d_π orbitals are degenerate. In $FeP(Im)_2^+$, the D_{4h} symmetry of FeP is broken by the imidazoles, so these are responsible for the energy splitting between d_{xz} and d_{yz}. A small perturbation such as twisting of the imidazoles is enough to change the occupation of the d_π orbitals. Not only small rotations of the singly occupied *d*-orbital, but also sudden 90° switches between d_{xz} and d_{yz} are observed. This shows that the two configurations still are nearly degenerate, despite the small asymmetry introduced by the imidazoles.

As already mentioned, the d-hole for $FeP(Im)_2^+$ is parallel to the imidazole plane yielding large spin densities at the C_β positions nearest to the imidazole plane (see Figure 6a). For $FeP(Im)_2^+$ in the gas phase, density functional theory strongly indicates that the parallel occupation is lower in energy. Calculations with both the BP and B3LYP functionals with both SV(P) and TZVP basis sets yield the same orientation as in Figure 6a. All four combinations also show the perhaps surprising switch to perpendicular orientation upon 180° rotation of one of the imidazoles, as seen in Figure 6c. This not in agreement with the general trend observed for heme systems.[79] One possible reason for the discrepancy might be the fact that DFT, being a single reference method, might have difficulties in accurately describing near-degenerate situations.

There is, however, no obvious reason to doubt the situation depicted in Figure 6a. The unsubstituted model does not represent real hemes that well, being too symmetric. The near degeneracy of d_{xz} and d_{yz} seems to be further split in favor of the perpendicular orientation by the various heme porphyrin substitutents and environment effects, both unaccounted for in the gas-phase calculations on $FeP(Im)_2^+$. For heme *a*, we indeed obtain a d-orbital occupation perpendicular to the plane of the imidazoles, and as a consequence the largest spin density is found at the C_β positions farthest from the imidazole plane, as seen in Figures 2 and 5. Also, rotating one of the imidazoles so that both N-3's point in the same direction does not switch the d-orbital occupation, in contrast with the unsubstituted model.

To further elucidate the problem, we performed calculations on heme *b* of cytochrome b_5. Heme *b* is a good example of a real system with both of its N-3 nitrogens on the same side, as in Figure 6c. We performed a BP/SV(P) single-point calculation on the crystal structure of heme *b*, taken from the Protein Data Bank under the identifier 1CYO.[80] The hydrogens were optimized using the MM+ force field.[81] The results were in accordance with the general trend for hemes, the singly occupied d-orbital being perpendicular to one of the axial imidazoles. The prediction by Shokhirev and Walker[79] was confirmed; the imidazole ligand defining the nodal plane is the one with a 71° angle to the meso carbons, not the 90° imidazole. This is probably due to the slightly shorter $Fe-N_{Im}$ bond length for the 71° imidazole.

When studying the spin distribution of systems where the axial ligand orientation is known, the results will probably benefit from turning back the axial ligands to their experimental torsion angles following an optimization of the molecular

(76) Sundholm, D. Unpublished.
(77) Meijer, E. J.; Sprik, M. *J. Chem. Phys.* **1996**, *105*, 8684.
(78) Turner, D. L.; Williams, R. J. P. *Eur. J. Biochem.* **1993**, *211*, 555.
(79) Shokhirev, N. V. ; Walker, F. A. *J. Biol. Inorg. Chem.* **1998**, *3*, 581.
(80) Durley, R. C. E.; Mathews, F. A. *Acta Crystallogr. D.* **1995**, *52*, 65.
(81) HYPERCHEM, Hypercube Inc., http://www.hyper.com/.

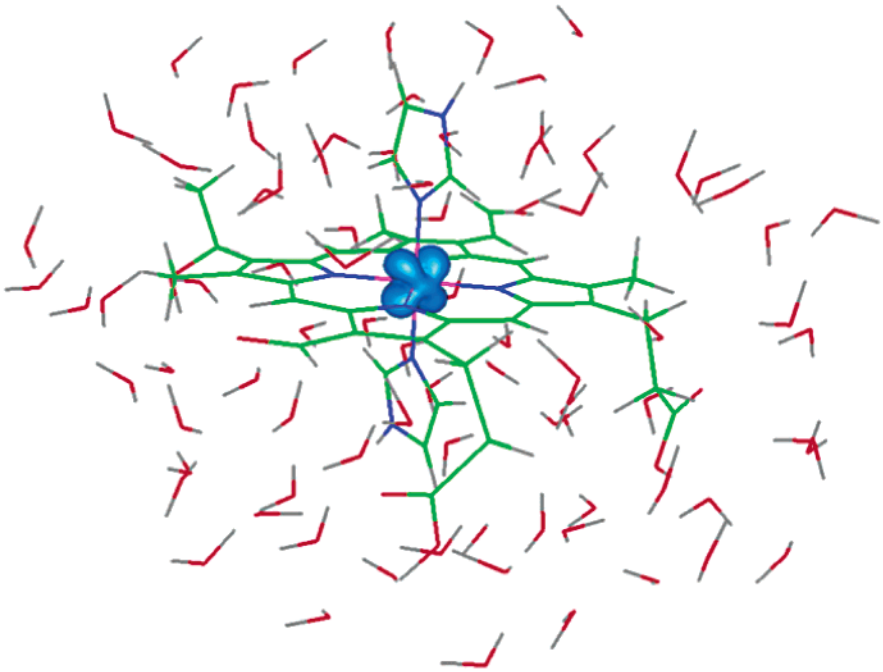

Figure 7. Heme *a* surrounded by 82 water molecules. The densest region of spin density is shown.

structure. As there is almost no energy barrier for the rotation, this procedure should not elicit any computational caveats. If the Fe−ligand bond lengths differ in the experimental structure and the lengths can be trusted, an adjustment of the optimized structure to reflect this might also be in place. In this way the most important effects of the surrounding protein backbone on the spin distribution can be accounted for, without increasing the model size.

The rotation barrier of the imidazoles is very low, and the axial ligands of the type II complexes are rotating fast.[7,82] The twisting of the imidazoles significantly perturb the spin distribution; such rather small changes in the geometry causes a surprisingly large modification of the spin density in the ring, giving some indication of the necessity of time averaging the spin density of the conformations accessible to the iron porphyrins.

It is emphasized that the molecular spin polarization around iron is present to the same degree regardless of how the rest of the spin sees fit to nest. We conclude that this spin polarization is a common feature of the studied low-spin iron porphyrins of type II.

III. E. Solvent Effects. The easiest method to consider solvent or protein effects is to apply some kind of continuum solvation model. In this work, we employed the COSMO model[83] as implemented in TURBOMOLE.[84] As seen in Figure 4, the accumulated spin-density maximum at 1.2 Å is approximately 0.02 electrons greater when the COSMO model with $\epsilon = 78$ is employed. In the protein, the dielectric constant is usually considered to be around 4.[85] The $\epsilon = 4$ curve lies nearly halfway between the $\epsilon = 78$ and vacuum curves. The spin density inside the virtual cavity is somewhat more contracted compared with the gas-phase calculation.

There is, however, a possible problem with the COSMO model, as well as with other continuum solvation models; the electron is prohibited from penetrating into the dielectricum around the molecule. This confinement of course inhibits a more diffuse electron distribution in the periphery, which also seems to affect the spin density near the porphyrin core.

The solvent effects were also studied by explicitly adding water around the heme. A single-point BP-UDFT/SV(P) calculation was performed on the optimized heme *a* embedded in 82 water molecules. The waters were relaxed using a molecular mechanics force field, MM+.[81] The heme *a* surrounded by the water molecules is shown in Figure 7. A contour plot of the densest region of the spin density is also depicted. In this case, the spin density becomes somewhat more diffuse as compared to the molecule in a vacuum. The accumulated spin-density maximum at 1.2 Å is approximately 0.02 electrons smaller when water is explicitly added around the heme. Thus, the effects from the dielectricum and from the explicit solvent molecules surrounding the heme to some extent cancel. After all, the effects from the surroundings are small and do not significantly affect the main features of the spin densities. Possible hydrogen bonding might be of importance for the spin densities, especially in the periphery, as recently shown by O'Malley.[86]

III. F. Functional and Basis-Set Effects. Spin densities obtained by performing BP-UDFT calculations qualitatively reproduce the results obtained using the more involved B3LYP-UDFT method. The locations of the regions of unpaired spin, as well as the shapes of the BP and B3LYP curves in Figure 3 are very similar, whereas the magnitude of the spin polarization differs somewhat. At the BP level, the spin-density distribution function reaches a local maximum of 0.9 electrons at a distance of about 1.2 Å from the iron, compared with 1.0 electrons according to the B3LYP calculations.

Uncertainties originating from the density functional are significantly larger than those due to basis-set effects, as well

(82) Maréchal, J. D.; Maseras, F.; Lledos, A.; Mouawad, L.; Perahia, D. *Chem. Phys. Lett.* **2002**, *353*, 379.
(83) Klamt, A.; Schüürmann, J. *Chem. Soc., Perkin Trans. 2* **1993**, *2*, 799.
(84) Schafer, A.; Klamt, A.; Sattel, D.; Lohrenz, J. C. W.; Eckert, F. *Phys. Chem. Chem. Phys. 2*, **2000**, *353*, 379.
(85) Simonson, T.; Perahia, D. *Proc. Natl. Acad. Sci. U.S.A.* **1995**, *92*, 1082.
(86) O'Malley, P. J. *J. Phys. Chem. B* **2001**, *105*, 11290.

as the treatment of the environment effects, discussed in section III. E. Previous calculations of hyperfine-interaction constants have show that the BP functional underestimates the spin density of π radicals.[87−88] On the other hand, Reiher et al.[89] found that the three parameters used in the parametrization of the B3LYP functional are not quite optimal for iron-containing compounds. The B3LYP functional tends to energetically favor high-spin states a bit too much, a fact noted also earlier.[90] To obtain spin states in agreement with experiment Reiher et al. used a somewhat smaller parameter for the Hartree−Fock exchange; the modified B3LYP functional yielded results in closer agreement with those obtained using the BP functional. Thus, for the low-spin hemes, the correct spin-density distribution functions probably lie somewhere between the BP and the B3LYP curves.

Basis-set effects are even smaller than the effect of the chosen functional. Calculations at SV(P) and TZVP yield almost quantitatively the same spin densities. The BP optimization calculation using TURBOMOLE's TZVPP basis set[60,64] showed that the basis-set limit for this property is almost reached; the accumulated spin-density curves obtained using TZVP and TZVPP basis sets practically coincide. Also the geometry is converged; the only difference is a small deviation in the rotation angle of the axial imidazoles, 10° vs 8° for the TZVP and TZVPP basis, respectively. The energy difference for a rotation angle of 2° is however comparable to the convergence criteria of the optimization run, so that there may in fact be no real difference. Environment effects not accounted for, like the surrounding protein, are likely to affect the rotation angle. Even so, the root-mean-square (RMS) deviation between the BP/TZVP and BP/TZVPP structures is only 0.04 Å.

Standard basis sets with contracted basis functions describing the core cannot consider the spin-polarization effects at the nuclei with sufficient accuracy. By decontracting the basis set and increasing the s and p basis, significant changes in the spin and electron densities at the nuclear positions are obtained. For example, the standard SV(P) basis set for iron yields a spin density at the nucleus that is of the same magnitude, but has opposite sign as compared to the spin density obtained using the fully decontracted SV(P) basis set. The spin polarization of the core was found to have little effect on the overall spin-density contribution and can, in that context, be omitted. A test calculation using an effective core potential on iron[91] further supports this notion; even the total lack of explicit core orbitals does not notably influence the total spin-density distribution.

Polarization functions in the basis set are not of critical importance either. A calculation with the split-valence basis without polarization functions, SV, performed just as well in describing the spin polarization as did the larger basis sets.

A minimal STO-3G basis set[92,93] on H, C, N, and O and SV on Fe, was also tested with the BP functional. This basis set, finally, proved to be too small for an adequate description of the heme *a* model; considerable spin densities are localized to the oxygens of the substituents, reducing the total spin of the iron to roughly 0.7. The amount of β spin along the Fe−N bonds is less than 0.1 electron in this case. The artificial reduction of α spin on the iron supports the polarization picture for the presence of the β spin; a smaller α density on the iron also results in a reduced extent of β spin around it.

III. G. Spin Contamination. Spin contamination can occur when the state of a system is not purely composed of one spin state, that is, it contains contributions from higher-spin states. A large spin contamination indicates a failure of the computational method used. The whole concept of spin contamination within DFT is, however, questionable. Often the expectation value $\langle S^2 \rangle$ is used for calculating the spin contamination, but since it is based on a two-particle operator, its meaning in density functional theory is diffuse. Gräfenstein and Cremer[94] recently showed, however, that $\langle S^2 \rangle$ can be assigned at least some diagnostic value also within DFT, and this was therefore checked.

The amount of spin contamination is taken as the difference between $\langle S^2 \rangle$ and the ideal value of $S(S + 1)$. In the case of the low-spin $S = {}^1/_2$ systems treated here, $\langle S^2 \rangle$, assumed meaningful, should have a value of 0.75. The calculations presented have at most a value of 0.78, the B3LYP calculations consistently having a somewhat higher value than the analogous BP calculations. This check gives no reason for concern.

IV. Conclusions

The present density-functional-theory calculations of the spin density for low-spin bis-imidazole-ligated iron porphyrins of type II show that the integrated spin density at the iron atom is about one. Even though the molecule has a net excess of one α electron, there are significant regions with excess of β spin. Large areas with β spin are found just outside the iron along the Fe−N bonds, whereas α spin dominates in the region between the nitrogens and the pyrrole C_β atoms. At the C_{meso} atoms, there is a small excess of β spin. Excess of α spin is also found at the pyrrole C_β atoms and in the vinyl substituent. The sum of unpaired α and β spin amounts to about 1.3 electrons.

The BP and the B3LYP density functionals provide rather similar spin densities. The correct spin density probably lies between the BP and the B3LYP densities. The uncertainties originating from the treatment of the environment effects and the basis-set effects are smaller than the uncertainties due to the density functional.

For the heme with perpendicular imidazoles, the porphyrin ring is somewhat ruffled, whereas with parallel imidazoles planar structures are obtained. The ruffling of the porphyrin ring does not notably affect the main features of the spin density.

Solvent effects do not significantly change the spin-density distribution either. By surrounding the heme with water molecules the spin density becomes somewhat more diffuse, whereas by applying a continuum solvation model the spin density contracts. The solvent effects from the dielectricum and from the explicit waters to some extent cancel.

The DFT techniques presented can be used to bridge the gap between measured spectroscopic parameters and molecular/electronic structure determination. For example, EPR spectroscopic techniques are becoming increasingly sophisticated in

(87) Suter, H. U.; Pless, V.; Ernzerhof, M.; Engels, B. *Chem. Phys. Lett.* **1994**, *230*, 398.
(88) Barone, V. *J. Phys.* **1994**, *101*, 6834.
(89) Reiher, M.; Salomon, O.; Hess, B. A. *Theor. Chem. Acc.* **2001**, *107*, 48.
(90) Paulsen, H.; Duelund, L.; Winkler, H.; Toftlund, H.; Trautwein, A. X. *Inorg. Chem* **2001**, *40*, 2201.
(91) Dolg, M.; Wedig, U.; Stoll, H.; Preuss, H. *J. Chem. Phys.* **1987**, *86*, 866.
(92) Hehre, W. J. ; Stewart, R. F.; Pople, J. A. *J. Chem. Phys.* **1969**, *51*, 2657.
(93) Hehre, W. J.; Ditchfield, R.; Stewart, R. F.; Pople, J. A. *J. Chem. Phys.* **1970**, *52*, 2769.
(94) Grafenstein, J.; Cremer, D. *Mol. Phys.* **2001**, *99*, 981.

the measurement of more accurate and precise values of hyperfine coupling constants and *g*-values. However, the experimentalist's ultimate goal is to use these improved data to obtain descriptive electronic and molecular structural information. This cannot be done without correspondingly sophisticated calculations which can be used to interpret the experimental data. The quality of the structures and spin-density distributions calculated here provide the means to meaningfully interpret and compare experimentally measured spectroscopic parameters.

Even though we have concentrated our present study on hemes, the results might also assist the interpretation of ESR and NMR spectra of other low-spin transition-metal systems; there is no reason to suspect that such a large spin polarization is present only in the types of systems studied here. It would in fact be surprising if further studies would not find this to be quite a general feature of transition-metal systems. However, a comparison of the spin densities obtained for type III hemes[95] with the present spin-density distributions shows that the spin density in type II and type III hemes apparently differs considerably.

The spin densities obtained in our calculations are mainly localized around the iron which is in good agreement with ESR and NMR spectroscopic data, whereas we have recently shown that the charge-density difference upon reduction of heme *a* is completely dispersed all over the heme.[52] Thus, the spatial distributions of the spin density and of the change in the charge density upon reduction are very different. A correlation between the two observables can nevertheless be noted; the spin polarization regions around the nitrogens are seen as charge polarization regions in the heme oxidation/reduction cycle.

Acknowledgment. We thank Dr. H. Konschin for useful discussions. M.P.J. and D.S. thank Professor R. Ahlrichs for a copy of TURBOMOLE and Professor P. Pyykkö for generous support. We acknowledge the support from the European research training network on "Molecular Properties and Molecular Materials" (MOLPROP) contract No. HPRN-2000-00013 (D.S.), the University of Helsinki's Research Funds (D.S.), the Sigrid Jusélius Foundation (M.W.), and the Academy of Finland. CSC - Scientific Computing Ltd. provided ample computer time for the most demanding calculations.

Note Added in Proof. After submitting the manuscript we were informed that quantitative and systematic calculations of NMR spectra of paramagnetic molecules at both ab initio and density-functional levels of theory have been performed.[100]

Supporting Information Available: Optimizations (PDF and text). This material is available free of charge via the Internet at http://pubs.acs.org.

JA026523J

(95) Ghosh, A.; Gonzales, E.; Vangberg, T. *J. Phys. Chem. B* **1999**, *103*, 1363.
(96) http://www.rcsb.org/pdb/.
(97) Laaksonen, L. *J. Mol Graphics* **1992**, *10*, 33.
(98) Bergman, D. L.; Laaksonen, L.; Laaksonen *J. Mol. Graphics Modell.* **1997**, *15*, 301.
(99) Laaksonen, http://www.csc.fi/gopenmol/.
(100) Rinkevicius, Z.; Vaara, J.; Telyatnyk, L.; Vahtras, O. Manuscript submitted to *J. Chem. Phys.*